Glacial cold-water coral growth in the Gulf of Cádiz:

Implications of increased palaeo-productivity

Claudia Wienberg[a,*], Norbert Frank[b], Kenneth N. Mertens[c], Jan-Berend Stuut[d,a],

Margarita Marchant[e], Jan Fietzke[f], Furu Mienis[a,d], Dierk Hebbeln[a]

[a] *Center for Marine Environmental Sciences (MARUM), University of Bremen, Leobener Str., 28359 Bremen, Germany*

[b] *Laboratoire des Sciences du Climat et de l'Environnement (LSCE), Bât.12, Avenue de la Terrasse, F-91198 Gif-sur-Yvette, France*

[c] *Research Unit Palaeontology (RUP), Ghent University, Krijgslaan 281 S8, 9000 Ghent, Belgium*

[d] *Royal Netherlands Institute for Sea Research (NIOZ), Landsdiep 4, 1797 SZ t'Horntje (Texel), The Netherlands*

[e] *Departamento de Zoología, Facultad de Ciencias Naturales y Oceanográficas, Universidad de Concepción, Casilla 160-C, Concepción, Chile*

[f] *Leibniz-Institute of Marine Sciences, IFM-GEOMAR, Wischhofstr. 1-3, 24148 Kiel, Germany*

* *Corresponding author. Tel: +49 421 21865652; Fax: +49 421 2189865652*
E-mail address: cwberg@marum.de (C. Wienberg)

1   **ABSTRACT**

2   A set of 40 Uranium-series datings obtained on the reef-forming scleractinian cold-water

3   corals *Lophelia pertusa* and *Madrepora oculata* revealed that during the past 400 kyr their

4   occurrence in the Gulf of Cádiz (GoC) was almost exclusively restricted to glacial periods.

5   This result strengthens the outcomes of former studies that coral growth in the temperate

6   NE Atlantic encompassing the French, Iberian and Moroccan margins dominated during

7   glacial periods, whereas in the higher latitudes (Irish and Norwegian margins) extended

8   coral growth prevailed during interglacial periods. Thus it appears that the biogeographical

9   limits for sustained cold-water coral growth along the NE Atlantic margin are strongly

10   related to climate change. By focussing on the last glacial-interglacial cycle, this study shows

11   that palaeo-productivity was increased during the last glacial. This was likely driven by the

12   fertilisation effect of an increased input of aeolian dust and locally intensified upwelling.

13   After the Younger Dryas cold event, the input of aeolian dust and productivity significantly

14   decreased concurrent with an increase in water temperatures in the GoC. This primarily

15   resulted in reduced food availability and caused a widespread demise of the formerly

16   thriving coral ecosystems. Moreover, these climate induced changes most likely caused a

17   latitudinal shift of areas with optimum coral growth conditions towards the northern NE

18   Atlantic where more suitable environmental conditions established with the onset of the

19   Holocene.

20

21   **Keywords**: cold-water corals; last glacial; productivity; aeolian dust; Gulf of Cádiz; NE Atlantic

22

23   **1. Introduction**

24   Along the NE Atlantic margin cold-water corals occur in a belt that extends from northern

25   Norway (Barents Sea, 70°N; Lindberg et al., 2007) down to NW Africa (off Mauritania, 16°N;

26   Colman et al., 2005). These ecosystems vary strongly with respect to their appearance,

27   structure and coral vitality. Large flourishing *Lophelia*-reefs occur along the Norwegian

28   margin. With a horizontal dimension of several hundred meters to kilometres they

29   developed to the largest known living cold-water coral reefs worldwide (Fosså et al., 2005).

30   Along the Irish margin cold-water corals are associated with coral mounds that vary in

31   height from a few metres up to 380 m being often densely covered by living coral colonies

32   (Wheeler et al., 2007, and refs. therein). Further to the south, cold-water corals mainly

33   occur as isolated colonies or accumulations of fossil corals in the Bay of Biscay (Reveillaud

34   et al., 2008), on seamounts (Duineveld et al., 2004) and within canyons along the Iberian

35   margin (Tyler et al., 2009), and on coral mounds along the NW African margin (Wienberg et

36   al., 2009).

37

38   Along with the geographic distribution, a distinct stratigraphic pattern regarding the

39   development of cold-water coral ecosystems along the NE Atlantic margin has been

40   observed during the last glacial-interglacial cycle. Reefs of Holocene age on the Norwegian

41   shelf started to develop after the retreat of glaciers at the termination of the last glacial

42   (Freiwald et al., 2004). The Irish coral mounds seem to be restricted to interglacials with a

43   very few exceptions (Dorschel et al., 2005; Eisele et al., 2008) and the latest re-

44   establishment of cold-water coral ecosystems appears to have been started after the

45   Younger Dryas (YD) cold reversal (Frank et al., 2009). To the south along the French, Iberian

46   and Moroccan margins, corals are suggested to have been widely distributed during the last

47   glacial (Schröder-Ritzrau et al., 2005; Wienberg et al., 2009). In actual fact, although the

48   Gulf of Cádiz (GoC) was recently identified to be an important cold-water coral site in the

49   temperate NE Atlantic, this area is at present mainly characterised by so-called 'coral

50   graveyards' with only very few living corals (Foubert et al., 2008; Wienberg et al., 2009).

51   Such current depauperation of live coral ecosystems might be explained by the recent

52   warm and oligotrophic conditions in the GoC forcing reduced food availability (Wienberg et

53   al., 2009). In addition, tidal currents and internal waves that have been identified to be

54 important hydrodynamic processes for supplying food particles to and through the coral

55 thickets (White et al., 2005; White et al., 2007) nowadays do not seem to play a major role

56 in the GoC (Wienberg et al., 2009). However, the widespread occurrence of fossil corals

57 suggests more favourable oceanographic conditions in the past. Indeed, initial datings

58 revealed that cold-water corals have been common in the GoC during the last glacial

59 (Wienberg et al., 2009).

60

61 The present study aims to refine and extend this observed stratigraphic pattern of coral

62 occurrence along the NE Atlantic margin by 40 Uranium-series datings of reef-forming

63 scleractinian cold-water corals from sediment cores retrieved in various areas of the GoC.

64 Moreover, it is intended to relate the prosperity and/or demise of cold-water corals in the GoC

65 to a distinct environmental and oceanographic setting that altered along with climate change.

66 Thus, we aim to identify the main forcing factors triggering the development of cold-water coral

67 ecosystems in the GoC.

68

69 **2. Regional setting**

70 The GoC is situated west of the Strait of Gibraltar, and thus connects the open North Atlantic

71 Ocean and the Mediterranean Sea (Fig. 1). It is bordered by the Iberian Peninsula and the NW

72 African coasts and extends from Cape St. Vincent at the southwestern tip of Portugal down to

73 the Moroccan Atlantic margin at 33°N (Mauritzen et al., 2001). The Iberian continental shelf

74 widens from ~15 km west of Faro to ~50 km further to the east (Garcia-Lafuente and Ruiz,

75 2007), which is similar to the width of the Moroccan shelf (<60 km; Mittelstaedt, 1991).

76

77 The deeper basin of the GoC is characterised by a widespread occurrence of diapiric ridges

78 and mud volcanoes (Somoza et al., 2003). Many of these mud volcanoes were identified to

79 be covered by fossil cold-water corals (Somoza et al., 2003; Wienberg et al., 2009). Further

80 conspicuous topographic features in the GoC are hundreds of coral mounds that are 20-30

81   m in height, and 50-200 m in length, and that are covered by fossil corals. They are

82   restricted to the Moroccan margin where they have been found in a water depth between

83   400 and 960 m (Foubert et al., 2008; Hebbeln et al., 2008; Wienberg et al., 2009). The coral

84   mounds are mainly arranged as clusters and are situated amidst mud volcanoes and on top

85   of diapiric ridges. Detailed knowledge about their origin, composition, and temporal

86   development is to date still lacking.

87

88   Present-day oceanographic circulation in the GoC is dominated by the exchange of water

89   masses between the Atlantic Ocean and the Mediterranean Sea (Ochoa and Bray, 1991).

90   The relatively cold Atlantic Inflow Water flows eastward along the Iberian margin partly

91   entering the Mediterranean Sea. It is composed of North Atlantic Surficial Water and North

92   Atlantic Central Water (NACW). The upper-thermocline NACW deepens from about 300 m

93   water depth close to the Strait of Gibraltar to about 600 m in the outer and southern parts

94   of the gulf (Ochoa and Bray, 1991; Mauritzen et al., 2001). Below this level occurs

95   Mediterranean Outflow Water (MOW). Flowing westwards through the Strait of Gibraltar,

96   the MOW prevails in the northern gulf where it flows between ~500 and 1 400 m water

97   depth above the North Atlantic Deep Water (NADW) (Ambar et al., 1999; Baringer and

98   Price, 1999) and acts as a strong contour current (García et al., 2009). It is characterised by

99   a permanent salinity maximum of ~36-37 and temperatures of 10.5 to 12°C (Fusco et al.,

100 2008). For the southern GoC along the Moroccan Atlantic margin information about its

101 hydrography is basically lacking (Machín et al., 2006). However, Pelegrí et al. (2005) suggests

102 the presence of MOW at 800 m. This assumption is supported by the presence of an

103 anticyclone or meddy close to the Moroccan shelf which implies at least some temporary

104 southward transport of MOW along the Moroccan margin (Carton et al., 2002).

105

106 Today, the GoC constitutes an oligotrophic system with diminished primary production in

107 the surface waters (Behrenfeld et al., 2005). Cold and productive upwelling is restricted to a

108   narrow band along the Portuguese coast (Garcia-Lafuente and Ruiz, 2007), and to the NW

109   African margin south of 31°N (Cape Ghir) (Mittelstaedt, 1991; Pelegrí et al., 2005). Due to a

110   prevailing anticyclonic circulation (Pelegrí et al., 2005), the basin of the GoC separates the

111   Iberian upwelling from the upwelling off NW Africa (Garcia-Lafuente and Ruiz, 2007).

112

113   **3. Material and methods**

114   **3.1 Core locations**

115   During three expeditions between 2003 and 2006, a set of ten coral-bearing sediment cores

116   was collected from various sites in the GoC (Table 1). The coring sites comprise two mud

117   volcanoes (Hespérides and Faro) along the Spanish margin and coral mounds along the

118   Moroccan margin which are situated on top of the prominent Renard Ridge and its

119   easternmost extension, the Pen Duick Escarpment. Finally, the southernmost core was

120   collected north of Meknes mud volcano (Fig. 1).

121

122   The sediment cores have a length between 2.2 m and 8.6 m and are made up of abundant

123   cold-water coral fragments embedded in a hemipelagic sediment matrix (Table 1). The

124   sediment cores collected from mud volcanoes along the Spanish margin only contain cold-

125   water corals in their upper parts, whereas the cores retrieved from coral mounds along the

126   Moroccan margin are characterised by the occurrence of coral fragments throughout the

127   sedimentary record.

128

129   To reconstruct oceanographic and environmental changes in the GoC during the last glacial-

130   interglacial cycle and to compare this with the temporal distribution pattern of cold-water

131   corals, sediment core GeoB 9064 (35°24.91'N, 06°50.72'W, 702 m water depth) was

132   selected for a multiproxy study (Fig. 1). Core GeoB 9064 was collected along the Moroccan

133   margin (RV *Sonne* cruise SO175) and has a total length of 5.4 m. Samples for the various

134   analyses were taken in 5-cm-intervals.

135

136   **3.2 U/Th age determination on coral fragments**

137   Forty fragments of the reef-forming scleractinian coral species *Madrepora oculata* and

138   *Lophelia pertusa* were sampled at different core depths from the sediment cores listed in

139   Table 1. Uranium-series measurements were performed using multi-collector ICP and

140   thermo-ionization mass spectrometry at IFM-GEOMAR (Kiel, Germany; Fietzke et al., 2005)

141   and at LSCE (Gif-sur-Yvette, France; Frank et al., 2004; Douville et al., 2010). Prior to

142   analyses, samples were carefully cleaned to remove contaminants from the fossil skeleton

143   surfaces according to procedures described by Fietzke et al. (2005) and Frank et al. (2004).

144   Isotope concentrations and ratios as well as the absolute dates on the cold-water corals are

145   provided in Table 2. Whole procedure blank values of this sample set were measured to be

146   around 2 pg for thorium (Th) and between 4 and 8 pg for uranium (U). Both values are

147   negligible compared to U- and Th-concentrations of the studied corals. The reproducibility

148   of mass spectrometric measurements was tested using international U standard materials

149   such as HU1 and NBL112, which provided identical values as the ones published by Fietzke

150   et al. (2005) and Frank et al. (2004).

151

152   **3.3 Analyses on core GeoB 9064**

153   **3.3.1 AMS radiocarbon dating**

154   Accelerator mass spectrometry (AMS) dating was performed at the Leibniz Laboratory for

155   Age Determinations and Isotope Research (University of Kiel, Germany; Nadeau et al.,

156   1997) and at the Poznań Radiocarbon Laboratory (Poznań, Poland). AMS ^{14}C dates were

157   determined on ~8 mg calcium carbonate of mixed planktonic foraminifera. All ages were

158   corrected for ^{13}C and a mean ocean reservoir age of 400 years (Bard, 1988). AMS ^{14}C ages

159 were converted to calendar years using the CALPAL 2007 Hulu software (Joeris and

160 Weninger, 1998) and are reported as calendar years before present (ka; Table 3).

161

162 **3.3.2 Stable oxygen isotopes**

163 The stable oxygen isotope ($\delta^{18}O$) composition of the planktonic foraminifera

164 *Neogloboquadrina pachyderma* (dex.) was measured with a Finnigan MAT 251 mass

165 spectrometer (Isotope Laboratory of the Department of Geosciences, University of Bremen,

166 Germany). The isotopic composition was measured on the CO_2 gas evolved by treatment with

167 phosphoric acid at a constant temperature of 75°C. A working standard (Burgbrohl CO_2 gas)

168 was applied, which has been calibrated against PDB by using the NBS18, 19 and 20 standards.

169 Consequently, all $\delta^{18}O$ data presented here are given relative to the PDB standard. Analytical

170 standard deviation was about ±0.07‰.

171

172 **3.3.3 Grain-size analysis and end-member modelling**

173 Grain sizes were measured on bulk and terrigenous material using a Malvern Instruments

174 Mastersizer 2000 (Hydraulic Research Laboratory, Borgerhout, Belgium), which determines

175 particle grain sizes between 0.26 µm and 2 046 µm grouped into 66 size classes. The

176 terrigenous sediment fraction was obtained by treating bulk sediment with H_2O_2 (30% at

177 85°C) and HCl (10% at 100°C) to remove organic carbon and calcium carbonate, respectively.

178 The sediments contained negligible amounts of biogenic opal, and microscopic analyses

179 revealed that the applied method successfully removed all biogenic constituents. Finally, the

180 samples were suspended in demineralised water by stirring and ultrasonic dispersion before

181 analysis.

182

183 The terrigenous fraction of deep-sea sediments in the ocean is considered a mixture of ice-

184 rafted, aeolian, and fluvial transported sediments. End-member modelling allows the

185   distinction between possible lithic subpopulations of the grain-size spectrum (Weltje, 1997)

186   that can be assigned to different sediment transport mechanisms (e.g., Stuut et al., 2002;

187   Holz et al., 2007). To estimate the minimum number of end-members (EM) required for a

188   satisfactory approximation of the data, the coefficients of determination were calculated.

189   These coefficients represent the proportion of the variance of each grain-size class that can

190   be reproduced by the approximated data. This proportion is equal to the squared

191   correlation coefficient (r^2) of input variables and their approximated values (Weltje, 1997;

192   Prins and Weltje, 1999). As the terrigenous sediment fraction from the southern GoC is

193   relatively fine-grained (<170 µm), the number of input variables for the end-member model

194   of core GeoB 9064 was reduced from 66 to 47 classes in the range of 0.29-170 µm.

195

196   **3.3.4. Planktonic foraminiferal assemblage**

197   The analysis for planktonic foraminiferal relative abundance counts is based on the

198   >150 µm fraction. For each sample a minimum of ~200 specimens were identified following

199   the taxonomy of planktonic foraminifera proposed by Hemleben et al. (1989). For

200   *Neogloboquadrina pachyderma* the relative abundances of right (dex.) and left (sin.) coiling

201   individuals were determined, and the two forms were treated as individual species. The

202   data are represented as percentages of total planktonic foraminiferal number.

203

204   **4. Results**

205   **4.1. U-series dating**

206   All selected coral fragments indicated minor to moderate physico-chemical alteration or

207   dissolution which may disturb U-series ages. Initial $\delta^{234}U_0$ values are variable and range

208   between 125.9±2.7‰ to 187.1±2.6‰ (Table 2, Fig. 2). Measured ^{232}Th concentrations are

209   small (<10 ng g^{-1}) for 75% of all samples (Fig. 2) but clearly specimens of *Madrepora oculata*

210   reveal more residual Th then *Lophelia pertusa* (Table 2). This is a consequence of the

211   cleaning procedure as the thinner polyps and more fragile skeleton of *M. oculata* is by far

212   more difficult to clean. However, Th contamination is negligible since in general the

213   ^{230}Th/^{232}Th activity ratios are >1 000.

214

215   Calculated U-series ages from all investigated coral sites in the GoC range from 9.2 ka to

216   more than 400 ka (Fig. 3). Two samples from core GeoB 12101 could not be dated due to

217   above equilibrium radioactive isotopic composition indicating U-series open system

218   behaviour. More than 90% of all obtained ages correspond to glacial periods (Marine

219   Isotope Stage (MIS) 2 back to MIS12), and 70% of these glacial coral ages cluster within the

220   last glacial (MIS2-4) (Fig. 3). With regard to the initial $\delta^{234}U_0$, it is evident that the scatter

221   increases largely beyond a coral age of 150 ka which is clearly indicative of increasing U-

222   series system opening (Thompson et al., 2003; Scholz et al., 2004; Frank et al., 2006;

223   Robinson et al., 2006). Consequently, those ages are less precise than the measured

224   uncertainty would suggest which has to be taken in consideration for our data

225   interpretation. Corals ages between 14 and 60 ka yield a mean initial $\delta^{234}U_0$ of 143.2±2.3‰

226   (n=22, 2σ standard deviation), which is slightly lower than measured in modern corals and

227   seawater (146.6-149.6‰; Delanghe et al., 2002; Robinson et al., 2004). Thus either corals

228   suffer from minor U-series system opening, and thus, preferential loss of ^{234}U, or the glacial

229   mean value of seawater was slightly lower than compared to today as suggested by Esat et

230   al. (1999). Overall we consider that within a range of 149±10‰ calculated ages are

231   representing the chronological ages of the corals within the uncertainty of measurement

232   (see also Stirling et al., 1998; Robinson et al., 2004; Esat and Yokoyama, 2006). However,

233   we are aware that a more detailed analysis of the U-series data and uncertainties

234   considering potential seawater U-isotopic variations, diagenetic alteration and U-series

235   system opening is needed to improve in particular the quality of coral ages beyond 150 ka.

236

4.2. Age model core GeoB 9064

237

238 The age model of core GeoB 9064 for the last ~40 kyr is based on six AMS ^{14}C age control

239 points and linear interpolation between these dates (Table 3, Fig. 4). The age model is

240 supported by the correlation of the $\delta^{18}O$ measurements of the record (showing heavy $\delta^{18}O$

241 values of 1.5-2.5‰ for the last glacial and light values of <1.0‰ for the Holocene; Fig. 4)

242 with the $\delta^{18}O$ record of the GRIP ice core (GRIP Members, 1993). The estimated average

243 sedimentation rate is ~16 cm ka^{-1} (Table 3). Highest sedimentation rates of 18-24 cm ka^{-1} occur

244 during MIS3 and the last deglaciation. Lowest sedimentation rates of 8-9 cm ka^{-1} are obtained for

245 MIS2 and the Holocene (Fig. 4).

246

4.3. Grain size distribution and source

247

248 The median grain size of the terrigenous (bulk) fraction of sediment core GeoB 9064 varies

249 between 5.71 µm (5.93 µm) and 12.03 µm (17.88 µm). The last glacial period and the Younger

250 Dryas (YD) cold event are characterised by relatively coarse sediment deposition. In contrast,

251 during the Holocene a distinct and continuous decrease of grain sizes is clearly visible (6-

252 9 µm) (Fig. 4). A three-end-member model was created (with r^2=0.77) to describe the grain

253 size data set of core GeoB 9064. The grain size distributions of the three end members are all

254 unimodal, well-sorted and have relatively fine modal grain sizes with 25 µm for EM1, 16 µm

255 for EM2, and 5 µm for EM3. Several sedimentological studies confirmed that aeolian

256 sediments deposited in the deep-sea close to the continent are coarser grained than

257 hemipelagic sediments with terrigenous sediments with mean grain sizes >6 µm being

258 generally attributed to aeolian transport, and sediments <6 µm to hemipelagic transport

259 (Ratmeyer et al., 1999; Prins et al., 2000). In addition, the mean modal sizes of present-day

260 aeolian dust, collected along a transect of the NW African coast (33°N to 12°S) vary between

261 8 µm and 42 µm (Stuut et al., 2005). Hence, for core GeoB 9064, the two coarsest end

262 members of the three-end-member model are considered to be of aeolian origin with EM1

interpreted as 'coarse' aeolian dust and EM2 as 'fine' aeolian dust. In contrast, EM3 is interpreted to result predominantly from fluvial input (Koopmann, 1981; Holz et al., 2007). During the last glacial, the aeolian content varies considerably between 30% and 60% and shows in particular during MIS3 rapid fluctuations. Close to the end of the last glacial (~17 ka), the aeolian content decreases before it increases again up to 60% during the YD. With the end of the YD (~11.5 ka), the proportion of the aeolian content on the total terrigenous fraction decreases continuously down to 25% (Fig. 4).

The EM1/EM2-ratio is considered as a measure for the relative wind intensity (Stuut et al., 2002). For core GeoB 9064, relatively high wind strength is indicated for the last glacial showing millennial-scale fluctuations. At ~22 ka, the wind conditions changed dramatically. Within a time period of 1.5 kyr, wind intensity decreased remarkably by 50% and stayed low during the entire Holocene (Fig. 4). This is deduced from a reduction of the content of 'coarse' aeolian dust (EM1) to almost zero, whereas the 'fine' aeolian dust (EM2) slightly increased towards the present.

4.4. Planktonic foraminiferal assemblage and abundance

The most abundant species in core GeoB 9064 is *Neogloboquadrina pachyderma* dex. (27.1%), followed by *Globigerinita glutinata* (21.1%), *Globigerina bulloides* (15.8%), and *Globorotalia inflata* (12.2%). Together with *Globigerinoides ruber* (5.2%), *Globorotalia scitula* (4.5%), and *N. pachyderma* sin. (4.5%), these species account on average for >90% of the total planktonic foraminifera.

Maximum relative abundances of *N. pachyderma* dex. is recorded during the last glacial, contributing up to 60% of the total planktonic foraminifera fauna. At the end of the last glacial (15.5-14.5 ka), its relative abundances decreased remarkably down to 10%, followed by an increase up to 40% during the YD. At the end of the YD (~11.5 ka), relative abundances of *N.*

290 *pachyderma* dex. significantly decreased down to <5% (Fig. 5). A similar trend is indicated for

291 *N. pachyderma* sin., although it shows comparably lower abundances below 18%. Another

292 abundant species during the last glacial was *G. glutinata* with relative abundances of 10-40%.

293 During the course of the Holocene, its contribution was rather low with minimum rates of

294 <10% except for the period between 10 and 8.5 ka, with relative abundances of up to 28%. An

295 opposite trend to the above mentioned species is observed for *G. bulloides*. Relatively low

296 abundance occurred during the last glacial (<20%), whereas during the Holocene, its relative

297 contribution to the total fauna increased to >20%. In particular between 8.5 and 2 ka, *G.*

298 *bulloides* was the most common species within the planktonic foraminiferal fauna with

299 relative abundance of 30-48%. Between 40 and 18 ka, abundances of *G. inflata* were below

300 20%, and increased up to 38% until the onset of the YD. During the Holocene, its abundances

301 varied between 8% and 20%. One distinct minimum (<10%) of *G. inflata* abundance is

302 indicated between 10 and 8.5 ka that mirrors the concomitant maxima of *G. glutinata*.

303 Contributions of *G. scitula* to the total fauna was rather moderate for most of the last glacial,

304 and decreased remarkably around 18 ka to <5%, and remained low thereafter (Fig. 5). During

305 the last glacial and until the end of the YD (~11.5 ka), *G. ruber* shows a low abundance of 0-

306 10% that increased to 10-25% during the Holocene. *Globigerinoides sacculifer* was even

307 absent during the last glacial. This species is exclusively found during the Holocene with

308 relative abundances of up to 7.5% (Fig. 5).

309

310 **5. Discussion**

311 **5.1. Glacial coral growth phases in the Gulf of Cádiz**

312 During the past years, much effort has been invested into dating cold-water corals from

313 various sites along the NE Atlantic margin. The most comprehensive data set of coral ages

314 exists for the Irish margin and reveals that coral growth in this area is restricted to the

315 Holocene and prior interglacial periods (Frank et al., 2005; Rüggeberg et al., 2007; de Haas

316 et al., 2009; Frank et al., 2009). In contrast, for coral sites south of 50°N the data set of coral

317 ages is rather scattered. However, the available dates suggest that the major phase of coral

318 growth along the French, Iberian and Moroccan margins coincide with the last glacial

319 period (Taviani et al., 1991; Schröder-Ritzrau et al., 2005; Wienberg et al., 2009).

320

321 For the GoC, it was shown that the reef-forming coral species *Lophelia pertusa* and

322 *Madrepora oculata* have been restricted to a period between 12 and 45 ka (Wienberg et al.,

323 2009). This preliminary result is confirmed by our data. In addition, the U/Th dates

324 presented here show that major phases of coral growth in the GoC are not solely restricted

325 to the last glacial but also to prior glacial periods (back to MIS12), whereas during

326 interglacials coral growth seems to be reduced or even absent (Fig. 2).

327

328 Most conspicuous is that the widespread decline of the coral ecosystems in the GoC during

329 the YD cold reversal (12.9–11.5 ka) corresponds to the re-start of coral mound formation on

330 Rockall Bank and the re-establishment of coral mound growth along the slopes of the

331 Porcupine Seabight at around 11 ka (Frank et al., 2009). Regarding this pattern, we suggest

332 that at the transition of the last glacial-interglacial, a latitudinal shift of areas with optimum

333 cold-water coral growth conditions towards the northern NE Atlantic occurred that was

334 most probably related to dramatic changes of the oceanographic and environmental

335 conditions caused by climate change. Moreover, this northward shift happened rapidly over

336 just a few hundreds of years and over a distance of 2 000-2 500 km (GoC to Irish margin).

337

338 Unfortunately, we still lack detailed understanding of the reproductive ecology and larval

339 dispersal mode of scleractinian cold-water corals. Histological studies show that the

340 cosmopolitan species *L. pertusa* exhibits an annual gametogenic cycle with spawning

341 around January/February (Waller and Tyler, 2005). The widespread occurrence of *L. pertusa*

342 and the rapid colonisation of man-made structures such as oil rigs (25 mm year^{-1}; Bell and

343   Smith, 1999), point to a dispersive planula larva being capable to remain in the water

344   column for several weeks.

345

346   **5.2. Driving factors for coral growth**

347   A combination of environmental and oceanographic conditions is required to promote a

348   sustained development of cold-water coral ecosystems. Cold-water corals require (1) hard

349   substrate to settle on, (2) protection against burial to grow, and (3) sufficient food supply.

350   Therefore, they predominate in areas where strong currents prevail that reduce deposition

351   of fine-grained sediments and supply large quantities of food (Roberts et al., 2006). Today,

352   thriving coral ecosystems occur in high concentrations in areas that are characterised by

353   enhanced primary production in the surface waters of eutrophic systems, allowing a

354   considerable part of the new production to be transported to the seafloor. In addition, tidal

355   currents and internal waves have been identified (1) to enhance concentrations of organic

356   matter at the shelf edge and (2) to transport fresh food particles to and through the cold-

357   water coral reefs (Frederiksen et al., 1992; White et al., 2005; White et al., 2007). Recently,

358   Dullo et al. (2008) indicated for the Celtic and Nordic margins that living cold-water corals

359   occur within the density envelope of sigma-theta (σ_Θ)=27.35-27.65 kg m^{-3} emphasising the

360   importance of physical boundary conditions. Finally, the world's most common cold-water

361   coral species *Lophelia pertusa* tends to be associated with oceanic water masses with a

362   temperature of 4-12°C (Roberts et al., 2006), and even up to 14°C in the Mediterranean Sea

363   (Taviani et al., 2005; Freiwald et al., 2009), salinities between 31.7 and 38.78 (Freiwald et

364   al., 2004; Davies et al., 2008), and oxygen concentrations of 4.3-7.2 ml l^{-1} (for the NE

365   Atlantic; Davies et al., 2008).

366

367   For the GoC, all these requirements must have been fulfilled during glacial periods as cold-

368   water corals were widespread during these times. During interglacial periods, these optimal

369   environmental and oceanographic conditions must have been changed dramatically

370   resulting in a widespread (gulf-wide) demise of the formerly thriving corals. As our obtained

371   coral ages mainly cluster within the last glacial (~70%), the environmental and

372   oceanographic changes of the GoC, focussing on the last glacial-interglacial cycle, are

373   discussed in detail to identify the main forcing factors for coral growth in the GoC.

374

375   **5.2.1 Effects of increased palaeo-productivity on cold-water coral growth**

376   Strong vertical fluxes of labile organic matter, as often found in eutrophic regions, result in

377   rich benthic fauna (e.g., De Stigter et al., 1998; Schmiedl et al., 2000; Fontanier et al., 2002).

378   In the NE Atlantic, seasonal algae blooms that sink rapidly to the deep-sea floor can even

379   have a positive effect on the reproductive biology of benthic invertebrates (Billett et al.,

380   1983; Thiel et al., 1989; Tyler et al., 1992), a relationship which is also hypothesised for

381   *Lophelia pertusa* and *Madrepora oculata* thriving along the Irish margin (Waller and Tyler,

382   2005). Thus, enhanced productivity is a pre-requisite for a sustained development of

383   healthy cold-water coral ecosystems. Indeed, regions with enhanced primary production as

384   deduced from satellite-based observations of the chlorophyll content in surface waters

385   (Behrenfeld et al., 2005) seem to mirror the recent distribution of thriving coral sites in the

386   NE Atlantic.

387

388   Certain species of planktonic foraminifera strongly depend on primary productivity in the

389   modern ocean (Hemleben et al., 1989), and hence downcore variations of the abundance of

390   planktonic foraminiferal species within sedimentary records can be applied to assess

391   palaeo-productivity conditions (e.g., Ivanova et al., 2003). In this context, the

392   environmental constraints of the most abundant foraminiferal species identified for the

393   GoC are reviewed in detail.

394

395   *Globigerina bulloides* mainly thrives in the surface mixed layer above the thermocline and

396   prefers relatively cold and nutrient-rich waters (e.g., Ganssen and Kroon, 2000; Chapman,

397   2010). Moreover, this species preferably occurs in areas along the Iberian and NW African

398   margins that are characterised by pronounced seasonal upwelling, and thus, by high

399   phytoplankton density and prey abundance (Salgueiro et al., 2008; Wilke et al., 2009). The

400   opportunistic and cosmopolitan species *Globigerinita glutinata* is also strongly associated

401   with the increase in productivity during spring bloom events in the North Atlantic

402   (Chapman, 2010). However, the distribution of this species is found to be even more

403   significantly associated with productivity than that of *G. bulloides*, which can be explained

404   by its diet that preferentially consists of diatoms (Bé and Tolderlund, 1971; Hemleben et al.,

405   1989; Schiebel et al., 2001). The sub-polar species *Neogloboquadrina pachyderma* dex.

406   prefers colder waters than *G. bulloides* (Bé and Tolderlund, 1971). Off the northern Iberian

407   margin, high percentages of this species have been related to increased productivity

408   generated by high river runoff (Salgueiro et al., 2008). In the GoC, *G. glutinata* and

409   *N. pachyderma* dex. clearly dominate the foraminiferal assemblage during the last glacial

410   with relative abundances of 55 to 75% (Fig. 5), thus pointing to rather nutrient-rich and cold

411   conditions compared to the following Holocene when both species account for only ~10%.

412   However, although *G. bulloides* is regarded as an indicator for nutrient enriched conditions

413   it shows an opposite trend compared to the other two species.

414

415   *Globorotalia inflata* is considered a non-upwelling species and high relative abundances of

416   this species in the North Atlantic coincide with oligotrophic waters (Pflaumann et al., 2003;

417   Salgueiro et al., 2008). The two surface-dwelling species *Globigerinoides ruber* and

418   *Globigerinoides sacculifer* show a preference towards oligotrophic conditions as well (e.g.,

419   Ivanova et al., 2003; Mohtadi et al., 2007). These species prefer warm and well stratified

420   surface waters (Duplessy et al., 1981; Stoll et al., 2007; Chapman, 2010). For the NE

421   Atlantic, a significant increase in the relative abundances of *G. sacculifer* is observed when

422   surface stratification is at a maximum and high sea surface temperatures prevail (Chapman,

423   2010). The significant increase of *G. ruber* and *G. sacculifer* after the YD cold event as found in

424   our record (Fig. 5) thus indicates such warm and well stratified conditions in the GoC during

425   the Holocene.

426

427   Taking all these findings for the NE Atlantic into account, *G. sacculifer*, *G. ruber* and *G.*

428   *inflata* are inferred to represent a low-productivity assemblage, whereas *G. glutinata*,

429   *G. bulloides* and *N. pachyderma* dex. are grouped as indicators for enhanced productivity.

430   Similar to the approach of Stoll et al. (2007), we calculated the ratio of both assemblages

431   and interpreted this ratio as an indicator of productivity (Fig. 4f), regardless of their affinity

432   to upwelling processes. This ratio clearly shows that during the last glacial palaeo-

433   productivity was overall enhanced in the GoC, which is in particular expressed by high

434   relative abundances of *G. glutinata* (Fig. 5). Following the end of the last glacial, this ratio

435   significantly changed towards more oligotrophic conditions (Fig. 4).

436

437   **5.2.2 Implications of frontal upwelling on glacial productivity in the GoC**

438   This pattern of eutrophic conditions during the last glacial and oligotrophic conditions

439   during the Holocene found for the GoC might be explained by a shift of the Azores Front

440   (Rogerson et al., 2004). The Azores Front marks a zone of strong hydrographic transition

441   associated with enhanced biological production caused by locally intense upwelling (Alves

442   and DeVerdière, 1999). Today, the easternmost extension of the Azores Front is situated at

443   30°N off the Moroccan margin (Gould, 1985; Schiebel et al., 2002), and hence, does not

444   penetrate into the GoC that extends from 37°N to 33°N (Fig. 1). But there is evidence that

445   the Azores Front shifted northward and thus penetrated eastward into the GoC prior to 16

446   ka and during the YD (Rogerson et al., 2004). Rogerson et al. (2004) indicated this glacial

447   shift of the Azores Front towards the GoC by high abundances of the planktonic foraminifer

448   *Globorotalia scitula* in their records. This deep-dwelling species (100-700 m water depth)

449   (Schiebel et al., 2002) is used as an indicator for cool surface waters and enhanced vertical

450   mixing at temperate latitudes (e.g., Thunell and Reynolds, 1984; Perez-Folgado et al., 2003).

451 Today *G. scitula* is found in high numbers in the Azores Front where upwelling causes high

452 productivity (Schiebel et al., 2002), but it is almost absent in the GoC (Rogerson et al.,

453 2004). The record of core GeoB 9064 shows that *G. scitula* is common prior to the Last

454 Glacial Maximum (LGM), but is rare throughout the Holocene (Fig. 5) pointing to enhanced

455 productivity during the last glacial caused by frontal upwelling.

456

457 **5.2.3 Fertilisation effect of aeolian dust**

458 Besides the effect of locally intensified upwelling that likely occurred in the GoC during the

459 last glacial also the high input of aeolian dust might have significantly enhanced glacial

460 productivity in the area. Grain size data from various sediment cores in the GoC, including

461 our data (Fig. 4), show that during the last glacial mean grain sizes were rather coarse

462 compared to the following Holocene (e.g., Rogerson et al., 2005; Voelker et al., 2006). Up to

463 now, these grain size variations have been primarily attributed to changes in the strength of

464 the prevailing bottom currents implying that bottom current strength was enhanced during

465 the last glacial probably caused by a shift and intensification of the MOW's flow pathway

466 (Schönfeld and Zahn, 2000; Rogerson et al., 2005; Voelker et al., 2006). Another common

467 finding for the GoC is a rather low Holocene sedimentation rate (e.g., Rogerson et al., 2005;

468 Voelker et al., 2006). Rogerson et al. (2005) estimated a Holocene accumulation rate that is

469 only one fifth of that of the last glacial, and thus is in agreement with our estimated rates

470 (Fig. 4). They assumed that this tremendous change in sedimentation rate was caused by a

471 higher sediment supply prior to the last deglaciation but without indicating the major

472 source of sediments supplied to the GoC.

473

474 However, this study shows that the variations in grain size and sedimentation rate as found

475 for the GoC are rather the result of changes in the source of the terrigenous sediments and

476 the amount of sediment input. Our grain size data clearly reveal that during the last glacial

477 the deposition of aeolian transported sediments prevailed in the GoC (Fig. 4). During this

478 time rather arid and cold conditions prevailed over the NW African continent (Gasse, 2000),

479 and the intensity of the northern trade winds, which transport the aeolian dust, was

480 enhanced especially from about 36°N to 24°N (Sarnthein et al., 1981; Hooghiemstra et al.,

481 1987; Moreno et al., 2002). This is supported by our record showing that wind strength off

482 Morocco (35°N) was significantly enhanced during the last glacial (Fig. 4). With the end of

483 the YD, the proportion of the aeolian content on the total terrigenous fraction decreased

484 continuously from 60 to 25% (Fig. 4), corresponding to the African humid period, which is

485 known to be characterised by a relatively humid and green Sahara with significantly lower

486 amounts of aeolian dust being produced (e.g., deMenocal et al., 2000; Gasse, 2000). The

487 African humid period terminated at 5.5 ka and the area of the Saharan desert returned to a

488 state of hyperarid conditions (deMenocal et al., 2000). However, wind strength remained

489 relatively low compared to the strong glacial trade winds (Hooghiemstra et al., 1987) and

490 dust fluxes have been estimated to be today 2-4 times lower compared to the LGM

491 (Grousset et al., 1998). Also our data show no significant increase of the input of aeolian

492 dust in the GoC after 5.5 ka until today (Fig. 4).

493

494 The large input of aeolian dust during the last glacial coincides with a prosperous cold-

495 water coral community in the GoC (Fig. 4). The link between dust input and coral prosperity

496 was probably established by a simple fertilisation effect. During periods of enhanced

497 Saharan dust input over the NE Atlantic, the supply of iron and manganese to the surface

498 ocean is enhanced as well (de Jong et al., 2007) which promotes primary production in the

499 surface waters (e.g., Boyd et al., 2000), and as a consequence, also might increase food

500 availability for the bathyal cold-water corals.

501

502 **5.2.4 Limitation of water temperatures on the prosperity of cold-water corals**

503 The planktonic foraminiferal abundance data of core GeoB 9064 is consistent with the

504 thermal history of the LGM and deglaciation. The general warming of the North Atlantic at

505   the transition from the last glacial to the Holocene is reflected by a considerable increase in

506   the abundance of *G. ruber* and *G. sacculifer* and a concurrent decrease in abundance of *N.*

507   *pachyderma* dex., which is even more pronounced after the YD cold reversal (Fig. 5). This

508   pattern is in agreement with other foraminiferal fauna records from the GoC (Sierro et al.,

509   1999; Rogerson et al., 2004). The change from rather cool towards warm surface waters

510   after the end of the YD was most likely accompanied by a change in subsurface

511   temperatures in intermediate water depths, thus having an impact on the bathyal cold-

512   water corals. Regarding the average temperatures of the intermediate water masses

513   prevailing in the GoC (NACW: ~12°C, Ait-Ameur and Goyet, 2006; MOW: 10.5-12°C, Fusco et

514   al., 2008), it becomes obvious that at least today water temperatures are at the very upper

515   tolerance for reef-forming scleractinian cold-water corals such as *Lophelia pertusa* (12°C;

516   Roberts et al., 2006). Moreover, dendrophylliid coral species that prefer rather warm

517   conditions compared to *L. pertusa* seem to have been more common during the late

518   Holocene (Wienberg et al., 2009).

519

520   **6. Conclusion**

521   This study clearly shows that the occurrence of cold-water corals in the GoC is dominant

522   within the last glacial and prior glacial periods and that hardly any cold-water corals exist in

523   this region during interglacials. Moreover, it could be identified that at the end of the YD

524   cold event a shift from eutrophic to oligotrophic and warm conditions have been

525   responsible for the demise of the formerly thriving coral ecosystems. The enhanced

526   productivity conditions during the last glacial have been most probably caused by (1) an

527   enhanced input of aeolian dust and (2) a shift of the Azores Fronts towards the GoC causing

528   locally intense upwelling. Both factor supported enhanced primary productivity in the GoC,

529   and thus resulted in enhanced food availability for the corals. By comparing our data set for

530   the GoC with coral ages from the Norwegian and Irish margins that reveal a sustained

531   prosperity of coral ecosystems right after the YD, it appears that a northward shift of areas

532   with optimum cold-water coral growth conditions took place during the transition from the

533   last glacial to the recent interglacial. The cold-water corals responded very rapidly to

534   climate change over just a few hundreds of years, and it is most likely that in the course of

535   global warming going along with dramatic changes in the environmental setting this

536   northward trend will further continue.

537

554   **References**

555   *Ait-Ameur, N., Goyet, C., 2006. Distribution and transport of natural and anthropogenic CO_2 in the Gulf of Cádiz.*
556   *Deep-Sea Res. II 53, 1329–1343.*
557   *Alves, M., DeVerdière, A.C., 1999. Instability dynamics of a subtropical jet and applications to the Azores Front*
558   *current system: Eddydriven mean flow. J. Physic. Oceanogr. 29, 837-864.*
559   *Ambar, I., Armi, L., Bower, A., Ferreira, T., 1999. Some aspects of time variability of the Mediterranean outflow.*
560   *Deep-Sea Res. 26A, 1109-1136.*
561   *Bard, E., 1988. Correction of accelerator mass spectrometry ^{14}C ages measured in planktonic foraminifera:*
562   *Paleoceanographic implications. Paleoceanography 3, 635-645.*
563   *Baringer, M.O., Price, J.F., 1999. A review of the physical oceanography of the Mediterranean outflow. Mar.*
564   *Geol. 155, 63-82.*
565   *Bé, A.W.H., Tolderlund, D.S., 1971. Distribution and ecology of living planktonic foraminifera in surface waters of*
566   *the Atlantic and Indian Oceans. In: Funel, B.M., Riedel, W.R. (Eds.), The Micropaleontology of Oceans.*
567   *Cambridge University Press, pp. 105-149.*
568   *Behrenfeld, M.J., Boss, E., Siegel, D.A., Shea, D.M., 2005. Carbon-based ocean productivity and phytoplankton*
569   *physiology from space. Glob. Biogeochem. Cycl. 19, GB1006, doi:1010.1029/2004GB002299.*
570   *Bell, N., Smith, J.E., 1999. Coral growing on North Sea oil rigs. Nature 402, 601.*
571   *Billett, D.S.M., Lampitt, R.S., Rice, A.L., Mantoura, R.F.C., 1983. Seasonal sedimentation of phytoplankton to the*
572   *deep-sea benthos. Nature Geosci. 302, 520-522.*
573   *Boyd, P.W., Watson, A.J., Law, C.S., Abraham, E.R., Trull, T., Murdoch, R., Bakker, D.C.E., Bowie, A.R., Buesseler,*
574   *K.O., Chang, H., Charette, M., Croot, P., Downing, K., Frew, R., Gall, M., Hadfield, M., Hall, J., Harvey, M.,*
575   *Jameson, G., LaRoche, J., Liddicoat, M., Ling, R., Maldonado, M.T., McKay, R., Nodder, S., Pickmere, S.,*
576   *Pridmore, R., Rintoul, S., Safi, K., Sutton, P., Strzepek, R., Tanneberger, K., Turner, S., Waite, A., Zeldis, J., 2000.*

577   *A mesoscale phytoplankton bloom in the polar Southern Ocean waters stimulated by iron fertilization. Nature*
578   *407, 695-702.*

579 Carton, X., Chérubin, L., Paillet, J., Morel, Y., Serpette, A., Le Cann, B., 2002. Meddy coupling with a deep cyclone
580   in the Gulf of Cádiz. J. Mar. Syst. 32, 13-42.

581 Chapman, M.R., 2010. Seasonal production pattern of planktonic foraminifera in the NE Atlantic Ocean:
582   Implications for paleotemperature and hydrographic reconstructions. Paleoceanography 25, PA1101,
583   doi:10.1029/2008PA001708.

584 Colman, J.G., Gordon, D.M., Lane, A.P., Forde, M.J., Fitzpatrick, J., 2005. Carbonate mounds off Mauritania,
585   Northwest Africa: status of deep-water corals and implications for management of fishing and oil exploration
586   activities. In: Freiwald, A., Roberts, J.M. (Eds.), Cold-water Corals and Ecosystems. Springer, Heidelberg, pp.
587   417-441.

588 Davies, A.J., Wisshak, M., Orr, J.C., Roberts, J.M., 2008. Predicting suitable habitat for the cold-water coral
589   Lophelia pertusa (Scleractinia). Deep-Sea Res. I 55, 1048-1062.

590 de Haas, H., Mienis, F., Frank, N., Richter, T.O., Steinbacher, R., de Stigter, H., van der Land, C., van Weering,
591   T.C.E., 2009. Morphology and sedimentology of (clustered) cold-water coral mounds at the south Rockall
592   Trough margins, NE Atlantic Ocean. Facies 55, 1-26.

593 de Jong, J.T.M., Boyé, M., Gelado-Caballero, M.D., Timmermans, K.R., Veldhuis, M.J.W., Nolting, R.F., van den
594   Berg, C.M.G., de Baar, H.J.W., 2007. Inputs of iron, manganese and aluminium to surface waters of the
595   Northeast Atlantic Ocean and the European continental shelf. Mar. Chem. 107, 120-142.

596 De Stigter, H.C., Jorissen, F.J., Vand der Zwaan, G.J., 1998. Bathymetric distribution and microhabitat partitioning
597   of live (Rose Bengal stained) benthic foraminifera along a shelf to deep sea transect in the southern Adriatic
598   Sea. J. Foram. Res. 28, 40-65.

599 Delanghe, D., Bard, E., Hamelin, B., 2002. New TIMS constraints on the uranium-238 and uranium-234 in
600   seawaters from the main ocean basins and the Mediterranean Sea. Mar. Chem. 80, 79-93.

601 deMenocal, P., Ortiz, J., Guilderson, T., Adkins, J., Sarnthein, M., Baker, L., Yarusinsky, M., 2000. Abrupt onset
602   and termination of the African Humid Period:: rapid climate responses to gradual insolation forcing. Quat. Sci.
603   Rev. 19, 347-361.

604 Dorschel, B., Hebbeln, D., Rüggeberg, A., Dullo, W.-C., 2005. Growth and erosion of a cold-water coral covered
605   carbonate mound in the Northeast Atlantic during the Late Pleistocene and Holocene. Earth Planet. Sci. Lett.
606   233, 33-44.

607 Douville, E., Sallé, E., Frank, N., Eisele, M., Pons-Branchu, E., Ayrault, S., 2010. Rapid and accurate Th-U dating of
608   ancient carbonates using Inductively Coupled Plasma-Quadrupole Mass Spectrometry. Chem. Geol. 272, 1-11.

609 Duineveld, G.C.A., Lavleye, M.S.S., Berghuis, E.M., 2004. Particle flux and food supply to a seamount cold-water
610   coral community (Galicia Bank, NW Spain). Mar. Ecol. Prog. Ser. 277, 13-23.

611 Dullo, C., Flögel, S., Rüggeberg, A., 2008. Cold-water coral growth in relation to the hydrography of the Celtic and
612   Nordic European continental margin. Mar. Ecol. Prog. Ser. 371, 165-176.

613 Duplessy, J.C., Bé, A.W., Blanc, P.L., 1981. Oxygen and carbon isotopic composition and biogeographic
614   distribution of planktonic foraminifera in the Indian Ocean. Palaeogeogr. Palaeoclimat. Palaeoecol. 33, 9-46.

615 Eisele, M., Hebbeln, D., Wienberg, C., 2008. Growth history of a cold-water coral covered carbonate mound -
616   Galway Mound, Porcupine Seabight, NE-Atlantic. Mar. Geol. 253, 160-169.

617 Esat, T.M., McCulloch, M.T., Chappell, J., Pillans, B., Omura, A., 1999. Rapid fluctuations in sea level recorded at
618   Huon Peninsula during the penultimate deglaciation. Science 283, 197-201.

619 Esat, T.M., Yokoyama, Y., 2006. Variability in the uranium isotopic composition of the oceans over glacial-
620   interglacial timescales. Geochim. Cosmochim. Acta 70, 4140-4150.

621 Fietzke, J., Liebetrau, V., Eisenhauer, A., Dullo, W.-C., 2005. Determination of uranium isotope ratios by multi-
622   static MIC-ICP-MS: method and implementation for precise U- and Th-series isotopes. J. Anal. Atomic Spectrom.
623   20, 395-401.

624 Fontanier, C., Jorissen, F.J., Licari, L., Alexandre, A., Anshutz, P., Carbonel, P., 2002. Live benthic foraminiferal
625   faunas from the Bay of Biscay: faunal density, composition, and microhabitats. Deep-Sea Res. I 49, 751-785.

626 Fosså, J.H., Lindberg, B., Christensen, O., Lundälv, T., Svellingen, I., Mortensen, P.B., Alsvag, J., 2005. Mapping of
627   Lophelia reefs in Norway: experiences and survey methods. In: Freiwald, A., Roberts, J.M. (Eds.), Cold-water
628   Corals and Ecosystems. Springer, Heidelberg, pp. 359-391.

629 Foubert, A., Depreiter, D., Beck, T., Maignien, L., Pannemans, B., Frank, N., Blamart, D., Henriet, J.-P., 2008.
630   Carbonate mounds in a mud volcano province off north-west Morocco: key to processes and controls. Mar.
631   Geol. 248, 74-96.

632 Frank, N., Paterne, M., Ayliffe, L., van Weering, T.C.E., Henriet, J.-P., Blamart, D., 2004. Eastern North Atlantic
633   deep-sea corals: tracing upper intermediate water $\Delta^{14}C$ during the Holocene. Earth Planet. Sci. Lett. 219, 297-
634   309.

635 Frank, N., Lutringer, A., Paterne, M., Blamart, D., Henriet, J.-P., van Rooij, D., van Weering, T.C.E., 2005. Deep-
636   water corals of the northeastern Atlantic margin: carbonate mound evolution and upper intermediate water
637   ventilation during the Holocene. In: Freiwald, A., Roberts, J.M. (Eds.), Cold-water Corals and Ecosystems.
638   Springer, Heidelberg, pp. 113-133.

639 Frank, N., Turpin, L., Cabioch, G., Blamart, D., Tressens-Fedou, M., Colin, C., Jean-Baptiste, P., 2006. Open system
640   U-series ages of corals from a subsiding reef in New Caledonia: Implications for sea level changes, and
641   subsidence rate. Earth Planet. Sci. Lett. 249, 274-289.
642 Frank, N., Ricard, E., Lutringer-Paque, A., van der Land, C., Colin, C., Blamart, D., Foubert, A., Van Rooij, D.,
643   Henriet, J.-P., de Haas, H., van Weering, T.C.E., 2009. The Holocene occurrence of cold-water corals in the NE
644   Atlantic: Implications for coral carbonate mound evolution. Mar. Geol. 266, 129-142.
645 Frederiksen, R., Jensen, A., Westerberg, H., 1992. The distribution of scleratinian coral Lophelia pertusa around
646   the Faroe Islands and the relation to intertidal mixing. Sarsia 77, 157-171.
647 Freiwald, A., Fosså, J.H., Grehan, A., Koslow, T., Roberts, J.M., 2004. Cold-water Coral Reefs. UNEP-WCMC,
648   Biodiversity Series 22, Cambridge, UK, p. 84.
649 Freiwald, A., Beuck, L., Rüggeberg, A., Taviani, M., Hebbeln, D., R/V Meteor Cruise M70-1 participants, 2009. The
650   white coral community in the central Mediterranean Sea revealed by ROV surveys. Oceanography 22, 58-74.
651 Fusco, G., Artale, V., Cotroneo, Y., Sannino, G., 2008. Thermohaline variability of Mediterranean Water in the
652   Gulf of Cádiz, 1948-1999. Deep-Sea Res. I 55, 1624-1638.
653 Ganssen, G., Kroon, D., 2000. The isotopic signature of planktonic foraminifera from the NE Atlantic surface
654   sediments: implications for the reconstruction of past oceanic conditions. J. Geol. Soc. London 157, 693-699.
655 Garcia-Lafuente, J., Ruiz, J., 2007. The Gulf of Cádiz pelagic ecosystem: A review. Prog. Oceanogr. 74, 228-251.
656 García, M., Hernández-Molina, F.J., Llave, E., Stow, D.A.V., León, R., Fernández-Puga, M.C., Diaz del Río, V.,
657   Somoza, L., 2009. Contourite erosive features caused by the Mediterranean Outflow Water in the Gulf of Cádiz:
658   Quaternary tectonics and oceanographic implications. Mar. Geol. 257, 24-40.
659 Gasse, F., 2000. Hydrological changes in the African tropics since the Last Glacial Maximum. Quat. Sci. Rev. 19,
660   189-211.
661 Gould, W.J., 1985. Physical oceanography of the Azores Front. Prog. Oceanogr. 14, 167-190.
662 GRIP Members, 1993. Climate instability during the last interglacial period recorded in the the GRIP ice core.
663   Nature 364, 203-207.
664 Grousset, F.E., Parra, M., Bory, A., Martinez, P., Betrand, P., Shimmield, G., Ellam, R.M., 1998. Saharan wind
665   regimes traced by the Sr-Nd isotopic composition of subtropical Atlantic sediments: Last Glacial Maximum vs.
666   today. Quat. Sci. Rev. 17, 395-409.
667 Hebbeln, D., Wienberg, C., cruise participants, 2008. Report and preliminary results of RV Pelagia cruise
668   64PE284, Cold-water corals in the Gulf of Cádiz and on Coral Patch Seamount, Portimao - Portimao, 18.02.-
669   09.03.2008. University of Bremen, Reports of the Department of Geosciences (GeoB) No. 265, p. 90.
670 Hemleben, C., Spindler, M., Anderson, O.R., 1989. Modern Planktonic Foraminifera. Springer, New York, 363 pp.
671 Holz, C., Stuut, J.-B., Meggers, H., Rüdiger, H., 2007. Variability in terrigenous sedimentation processes off
672   northwest Africa and its relation to climatic changes: inferences from grain-size distributions of a Holocene
673   marine sediment record. Sediment. Geol. 202, 499-508.
674 Hooghiemstra, H., Bechler, A., Beug, H.-J., 1987. Isopollen maps for 18,000 years BP of the Atlantic offshore of
675   Northwest Africa: Evidence for paleowind circulation. Paleoceanography 2, 561-582.
676 Imbrie, J., Hays, J.D., Martinson, D.G., McIntyre, A., Mix, A.C., Morley, J.J., Pisias, N.G., Prell, W.L., Shackleton,
677   N.J., 1989. The orbital theory of Pleistocene climate: support from a revised chronology of the marine $\delta^{18}O$
678   record. In: Berger, A. (Ed.), Milankovitch and Climate. NATO ASI Series, Dordrecht, pp. 269-305.
679 Ivanova, E., Schiebel, R., Singh, A.D., Schmiedl, G., Niebler, H.-S., Hemleben, C., 2003. Primary production in the
680   Arabian Sea during the last 135000 years. Palaeogeogr. Palaeoclimat. Palaeoecol. 197, 61-82.
681 Joeris, O., Weninger, B., 1998. Extension of the ^{14}C calibration curve to ca. 40,000 cal BC by synchronizing
682   Greenland $^{18}O/^{16}O$ ice core records and North Atlantic foraminifera profiles: A comparison with U/Th coral
683   data. Radiocarbon 40, 495-504.
684 Koopmann, B., 1981. Sedimentation von Saharastaub im subtropischen Nordatlantik während der letzten 25.000
685   Jahre. Meteor Forschungsergeb. 35, 23-59.
686 Lindberg, B., Berndt, C., Mienert, J., 2007. The Fugløy Reef at 70°N; acoustic signature, geologic, geomorphologic
687   and oceanographic setting. Int. J. Earth Sci. 96, 201-213.
688 Machín, F., Pelegrí, J.L., Marrero-Díaz, A., Laiz, I., Ratsimandresy, A.W., 2006. Near-surface circulation in the
689   southern Gulf of Cádiz. Deep-Sea Res. II 53, 1161-1181.
690 Mauritzen, C., Morel, J., Paillet, J., 2001. On the influence of Mediterranean water on the central waters of the
691   North Atlantic Ocean. Deep-Sea Res. 44, 1543-1574.
692 Mittelstaedt, E., 1991. The ocean boundary along the northwest African coast: Circulation and oceanographic
693   properties at the sea surface. Prog. Oceanogr. 26, 307-355.
694 Mohtadi, M., Max, L., Hebbeln, D., Baumgart, A., Krück, N., Jennerjahn, T., 2007. Modern environmental
695   conditions recorded in surface sediment samples off W and SW Indonesia: Planktonic foraminifera and biogenic
696   compounds analyses. Mar. Micropaleontol. 65, 96-112.
697 Moreno, A., Cacho, I., Canals, M., Prins, M.A., Sánchez-Goñi, M.-F., Grimalt, J.O., Weltje, G.J., 2002. Saharan dust
698   transport and high-latitude glacial climatic variability: The Alboran Sea record. Quat. Res. 58, 318-328.
699 Nadeau, M.J., Schleicher, M., Grootes, P., Erlenkeuser, H., Gottolong, A., Mous, D.J.W., Sarnthein, M., Willkomm,
700   N., 1997. The Leibniz-Labor AMS facility of the Christian-Albrechts University, Kiel, Germany. Nucl. Instrum.
701   Methods Phys. Res. 123, 22-30.
702 Ochoa, J., Bray, N.A., 1991. Water mass exchange in the Gulf of Cádiz. Deep-Sea Res. 38 (S1), 5465-5503.

703 Pelegrí, J.L., Marrero-Díaz, A., Ratsimandresy, A., Antoranz, A., Cisneros-Aguirre, J., Gordo, C., Grísolia, D.,
704   Hernández-Guerra, A., Láiz, I., Martínez, A., Parrilla, G., Pérez-Rodriguez, P., Rodríguez-Santana, A., Sangrà, P.,
705   2005. Hydrographic cruises off northwest Africa: the Canary Current and the Cape Ghir region. J. Mar. Syst. 54,
706   39-63.
707 Perez-Folgado, M., Sierro, F.J., Flores, J.A., Cacho, I., Grimalt, J.O., Zahn, R., Shackleton, N.J., 2003. Western
708   Mediterranean planktonic foraminifera events and millennial climatic variability during the last 70 kyr. Mar.
709   Micropaleontol. 48, 49-70.
710 Pflaumann, U., Sarnthein, M., Chapman, M., d'Abreu, L., Funnell, B., Huels, M., Kiefer, T., Maslin, M., Schulz, H.,
711   Swallow, J., van Kreveld, S., Vautravers, M., Vogelsang, E., Weinelt, M., 2003. Glacial North Atlantic: sea-
712   surface conditions reconstructed by GLAMAP 2000. Paleoceanography 18, 1065.
713 Prins, M.A., Weltje, G.J., 1999. End-member modeling of siliciclastic grain-size distributions: the Late Quaternary
714   record of eolian and fluvial sediment supply to the Arabian Sea and its paleoclimatic significance. In: Harbaugh,
715   J., Watney, L., Rankey, G., Slingerland, R., Goldstein, R., Franseen, E. (Eds.), Numerical Experiments in
716   Stratigraphy: Recent Advances in Stratigraphic and Sedimentologic Computer Simulations. SEPM, pp. 91-111.
717 Prins, M.A., Postma, G., Cleveringa, J., Cramp, A., Kenyon, N.H., 2000. Controls on terrigenous sediment supply to
718   the Arabian Sea during the late Quaternary: the Indus Fan. Mar. Geol. 169, 327-349.
719 Ratmeyer, V., Balzer, W., Bergametti, G., Chiapello, I., Fischer, G., Wyputta, U., 1999. Seasonal impact of mineral
720   dust on deep-ocean particle flux in the eastern subtropical Atlantic Ocean. Mar. Geol. 159, 241-252.
721 Reveillaud, J., Freiwald, A., Van Rooij, D., Le Guilloux, E., Altuna, A., Foubert, A., Vanreusel, A., Olu-Le Roy, K.,
722   Henriet, J.-P., 2008. The distribution of scleractinian corals in the Bay of Biscay, NE Atlantic. Facies 54, 317-331.
723 Roberts, J.M., Wheeler, A.J., Freiwald, A., 2006. Reefs of the deep: The biology and geology of cold-water coral
724   ecosystems. Science 312, 543-547
725 Robinson, L.F., Belshaw, N.S., Henderson, G.M., 2004. U and Th concentrations and isotope ratios in modern
726   carbonates and waters from the Bahamas. Geochim. Cosmochim. Acta 68, 1777-1789.
727 Robinson, L.F., Adkins, J.F., Fernandez, D.P., Burnett, D.S., Wang, S.-L., Gagnon, A.C., Krakauer, N., 2006. Primary
728   U distribution in scleractinian corals and its implications for U series dating. Geochem. Geophysic. Geosyst. 7,
729   Q05022, doi, 10.1029/2005GC001138.
730 Rogerson, M., Rohling, E.J., Weaver, P.P.E., Murray, J.W., 2004. The Azores Front since the Last Glacial
731   Maximum. Earth Planet. Sci. Lett. 222, 779-789.
732 Rogerson, M., Rohling, E.J., Weaver, P.P.E., Murray, J.W., 2005. Glacial to interglacial changes in the settling
733   depth of the Mediterranean Outflow plume. Paleoceanography 20, PA3007, doi:3010.1029/2004PA001106.
734 Rüggeberg, A., Dullo, W.-C., Dorschel, B., Hebbeln, D., 2007. Environmental changes and growth history of a
735   cold-water carbonate mound (Propeller Mound, Porcupine Seabight). Int. J. Earth Sci. 96, 57-72.
736 Salgueiro, E., Voelker, A., Abrantes, F., Meggers, H., Pflaumann, U., Loncaric, N., González-Álvarez, R., Oliveira,
737   P., Bartels-Jónsdóttir, H.B., Moreno, J., Wefer, G., 2008. Planktonic foraminifera from modern sediments reflect
738   upwelling patterns off Iberia: Insights from a regional transfer function. Mar. Micropaleontol. 66, 135-164.
739 Sarnthein, M., Tetzlaff, G., Koopmann, B., Wolter, K., Pflaumann, U., 1981. Glacial and interglacial wind regimes
740   over the eastern tropical Atlantic and Northwest Africa. Nature 293, 193-196.
741 Schiebel, R., Waniek, J., Bork, M., Hemleben, C., 2001. Planktic foraminiferal production stimulated by
742   chlorophyll redistribution and entrainment of nutrients. Deep-Sea Res. I 48, 721-740.
743 Schiebel, R., Waniek, J., Zeltner, A., Alves, M., 2002. Impact of the Azores Front on the distribution of planktic
744   foraminifers, shelled gastropods and coccolithophorids. Deep-Sea Res. II 49, 4035-4050.
745 Schmiedl, G., de Bovée, F., Buscail, R., Charrière, B., Hemleben, C., Medernach, L., Picon, P., 2000. Trophic control
746   of benthic foraminiferal abundance and microhabitat in the bathyal Gulf of Lions, western Mediterranean Sea.
747   Mar. Micropaleontol. 40, 167-188.
748 Scholz, D., Mangini, A., Felis, T., 2004. U-series dating of diagenetically altered fossil reef corals. Earth Planet. Sci.
749   Lett. 218, 163-178.
750 Schönfeld, J., Zahn, R., 2000. Late Glacial to Holocene history of the Mediterranean Outflow. Evidence from
751   benthic foraminiferal assemblages and stable isotopes at the Portuguese margin. Palaeogeogr. Palaeoclimat.
752   Palaeoecol. 159, 85-111.
753 Schröder-Ritzrau, A., Freiwald, A., Mangini, A., 2005. U/Th-dating of deep-water corals from the eastern North
754   Atlantic and the western Mediterranean Sea. In: Freiwald, A., Roberts, J.M. (Eds.), Cold-water Corals and
755   Ecosystems. Springer, Heidelberg, pp. 691-700.
756 Sierro, F.J., Flores, J.A., Baraza, J., 1999. Late glacial to recent paleoenvironmental changes in the Gulf of Cadiz
757   and formation of sandy contourite layers. Mar. Geol. 155, 157-172.
758 Somoza, L., Diaz-del-Rio, V., Leon, R., Ivanov, M., Fernandez-Puga, M.C., Gardner, J.M., Hernandez-Molina, F.J.,
759   Pinheiro, L.M., Rodero, J., Lobato, A., 2003. Seabed morphology and hydrocarbon seepage in the Gulf of Cádiz
760   mud volcano area: Acoustic imagery, multibeam and ultra-high resolution seismic data. Mar. Geol. 195, 153-
761   176.
762 Stirling, C.H., Esat, T.M., Lambeck, K., McCulloch, M.T., 1998. Timing and duration of the Last Interglacial:
763   evidence for a restricted interval of widespread coral reef growth. Earth Planet. Sci. Lett. 160, 745-762.
764 Stoll, H.M., Arevalos, A., Burke, A., Ziveri, P., Mortyn, G., Shimizu, N., Unger, D., 2007. Seasonal cycles in biogenic
765   production and export in Northern Bay of Bengal sediment traps. Deep-Sea Res. II 54, 558-580.

766   *Stuut, J.-B.W., Prins, M.A., Schneider, R.R., Weltje, G.J., Jansen, J.H.F., Postma, G., 2002. A 300-kyr record of*
767   *aridity and wind strength in southwestern Africa: inferences from grain-size distributions of sediments on*
768   *Walvis Ridge, SE Atlantic. Mar. Geol. 180, 221-233.*
769   *Stuut, J.B., Zabel, M., Ratmeyer, V.H., P., Schefuß, E., Lavik, G., Schneider, R.R., 2005. Provenance of present-day*
770   *eolian dust collected off NW Africa: implications for deep-marine sediment studies. J. Geophys. Res. 110,*
771   *D04202.*
772   *Taviani, M., Bouchet, P., Metivier, B., Fontugne, M., Delibrias, G., 1991. Intermediate steps of southwards faunal*
773   *shifts testified by last glacial submerged thanatocoenoses in the Atlantic Ocean. Palaeogeography,*
774   *Palaeoclimatology, Palaeoecology 86, 331-338.*
775   *Taviani, M., Remia, A., Corselli, C., Freiwald, A., Malinverno, E., Mastrototaro, F., Savini, A., Tursi, A., 2005. First*
776   *geo-marine survey of living cold-water Lophelia reefs in the Ionian Sea (Mediterranean basin). Facies 50, 409-*
777   *417.*
778   *Thiel, H., Pfannkuche, O., Schriever, G., Lochte, K., Gooday, A.J., Hemleben, C., Mantoura, R.F.C., Turley, C.M.,*
779   *Patching, J.W., Riemann, F., 1989. Phytodetritus on the deep-sea floor in a central region of the Northeast*
780   *Atlantic. Biol. Oceanogr. 6, 203-239.*
781   *Thompson, W.G., Spiegelman, M.W., Goldstein, S.L., Speed, R.C., 2003. An open-system model for U-series age*
782   *determinations of fossil corals. Earth Planet. Sci. Lett. 210, 365-381.*
783   *Thunell, R., Reynolds, L., 1984. Sedimentation of planktonic foraminifera: Seasonal changes in species flux in the*
784   *Panama Basin. Micropaleontology 30, 243-262.*
785   *Tyler, B., Amaro, T., Arzola, R., Cunha, M.R., De Stigter, H., Gooday, A., Huvenne, V., Ingels, J., Kiriakoulakis, K.,*
786   *Lastras, G., Masson, D.G., Oliveira, A., Pattenden, A., Vanreusel, A., Van Weering, T.C.E., Vitorino, J., Witte, U.,*
787   *Wolff, G., 2009. Europe's Grand Canyon: Nazaré Submarine Canyon. Oceanography 22, 46-57.*
788   *Tyler, P.A., Harvey, R., Giles, L.A., Gage, J.D., 1992. Reproductive strategies and diet in deep-sea nuculanid*
789   *protobranchs (Bivalvia: Nuculoidea) from the Rockall Trough. Mar. Biol. 114, 571-580.*
790   *Voelker, A.H.L., Lebreiro, S.M., Schönfeld, J., Cacho, I., Erlenkeuser, H., Abrantes, F., 2006. Mediterranean*
791   *outflow strengthening during northern hemisphere coolings: A salt source for the glacial Atlantic. Earth Planet.*
792   *Sci. Lett. 245, 39-55.*
793   *Waller, R.G., Tyler, P.A., 2005. The reproductive biology of two deep-water, reef-building scleractinians from the*
794   *NE Atlantic Ocean. Coral Reefs 24, 514-522.*
795   *Weltje, G., 1997. End-member modeling of compositional data: Numerical-statistical algorithms for solving the*
796   *explicit mixing problem. Math. Geol. 29, 503-549.*
797   *Wheeler, A.J., Beyer, A., Freiwald, A., de Haas, H., Huvenne, V., Kozachenko, M., Olu-Le Roy, K., Opderbecke, J.,*
798   *2007. Morphology and environment of cold-water coral carbonate mounds on the NW European margin. Int. J.*
799   *Earth Sci. 96, 37-56.*
800   *White, M., Mohn, C., de Stigter, H., Mottram, G., 2005. Deep-water coral development as a function of*
801   *hydrodynamics and surface productivity around the submarine banks of the Rockall Trough, NE Atlantic. In:*
802   *Freiwald, A., Roberts, J.M. (Eds.), Cold-Water Corals and Ecosystems. Springer, Heidelberg, pp. 503-514.*
803   *White, M., Roberts, J.M., van Weering, T.C.E., 2007. Do bottom-intensified diurnal tidal currents shape the*
804   *alignment of carbonate mounds in the NE Atlantic? Geo-Mar. Lett. 27, 391-397.*
805   *Wienberg, C., Hebbeln, D., Fink, H.G., Mienis, F., Dorschel, B., Vertino, A., López Correa, M., Freiwald, A., 2009.*
806   *Scleractinian cold-water corals in the Gulf of Cádiz - first clues about their spatial and temporal distribution.*
807   *Deep-Sea Res. I 56, 1873-1893.*
808   *Wilke, I., Meggers, H., Bickert, T., 2009. Depth habitats and seasonal distributions of recent planktic foraminifers*
809   *in the Canary Islands region (29°N) based on oxygen isotopes. Deep-Sea Res. I 56, 89-106.*
810
811
812

813   **Figure 1. Map of the Gulf of Cádiz (GoC) showing the coring sites** (bathymetric data source:

814   GEBCO). Reference sediment core GeoB 9064 (black triangle) and coral-bearing sediment

815   cores (A-D). A: Hespérides mud volcano (GeoB 9018), B: Faro mud volcano (GeoB 9031, GeoB

816   9032), C: Renard Ridge (GeoB 9070, GeoB 12101, GeoB 12102, GeoB 12103, GeoB 12104,

817   M2004-02), D: north of Meknes mud volcano (GeoB 12106). Indicated are the reported

818   occurrences of fossil cold-water corals (after Wienberg et al., 2009). Lower left: photographs

819   showing characteristic 'coral graveyards' in the southern GoC, Moroccan margin (position is

820   indicated on the map as p1, p2) (images ©MARUM, Bremen).

821

822   **Figure 2**. **Initial U-isotopic ratios of cold-water corals (lower graph) and ^{232}Th concentration**

823   **(upper graph).** δ^{234}U is in almost all cases very close to present-day seawater (149.9‰: blue

824   dashed line; range of 149.9±10‰: light blue bar), except for the deepest sample in core GeoB

825   12104 (+38‰). ^{232}Th concentrations for 75% of all samples are below 10 ng g^{-1} (green dashed

826   line).

827   **Figure 3. ^{230}Th/U datings conducted on cold-water coral fragments collected in the GoC.**

828   AMS ^{14}C ages presented by Wienberg et al. (2009) are implemented. Note that solely reef-

829   forming species such as *Madrepora oculata* and *Lophelia pertusa* are considered showing

830   that >90% of all coral ages coincide with glacial periods. Marine Isotope Stages (MIS) are

831   indicated by grey bars based on SPECMAP δ^{18}O stack (Imbrie et al. 1989).

832

833   **Figure 4. Multi-proxy data of sediment core GeoB 9064.** (**a**) Estimated sedimentation rate,

834   (**b**) stable oxygen isotopes record (lower curve) compared with the GRIP ice core record

835   (upper curve) (**c**) median grain size (terrigenous and bulk sediment), (**d**) relative aeolian

836   input, (**e**) relative wind strength, and (**f**) productivity index based on the ratio of high- to

837   low-productivity planktonic foraminiferal assemblages. AMS ^{14}C dates obtained for core

838   GeoB 9064 are marked by black diamonds. For comparison, U/Th (squares; this study) and

839   AMS ^{14}C coral dates (triangles; Wienberg et al., 2009) obtained for the past 50 kyr are

840   implemented. Note that solely reef-forming species such as *Madrepora oculata* and

841   *Lophelia pertusa* are considered.

842

843   **Figure 5. The δ^{18}O record and planktonic foraminiferal abundance for sediment core GeoB**

844   **9064.** (**a**) δ^{18}O$_{N. pachyderma (dex.)}$, (**b**) *Neogloboquadrina pachyderma* (black: dex., grey: sin.), (**c**)

845   *Globigerinita glutinata*, (**d**) *Globigerina bulloides*, (**e**) *Globigerinoides ruber* (black) and

846   *Globigerinoides sacculifer* (grey), (**f**) *Globorotalia inflata*, (**g**) *Globorotalia scitula*. Younger

847   Dryas (YD) and Marine Isotope Stages (MIS) 2 and 3 are indicated.

848

849

Figure1
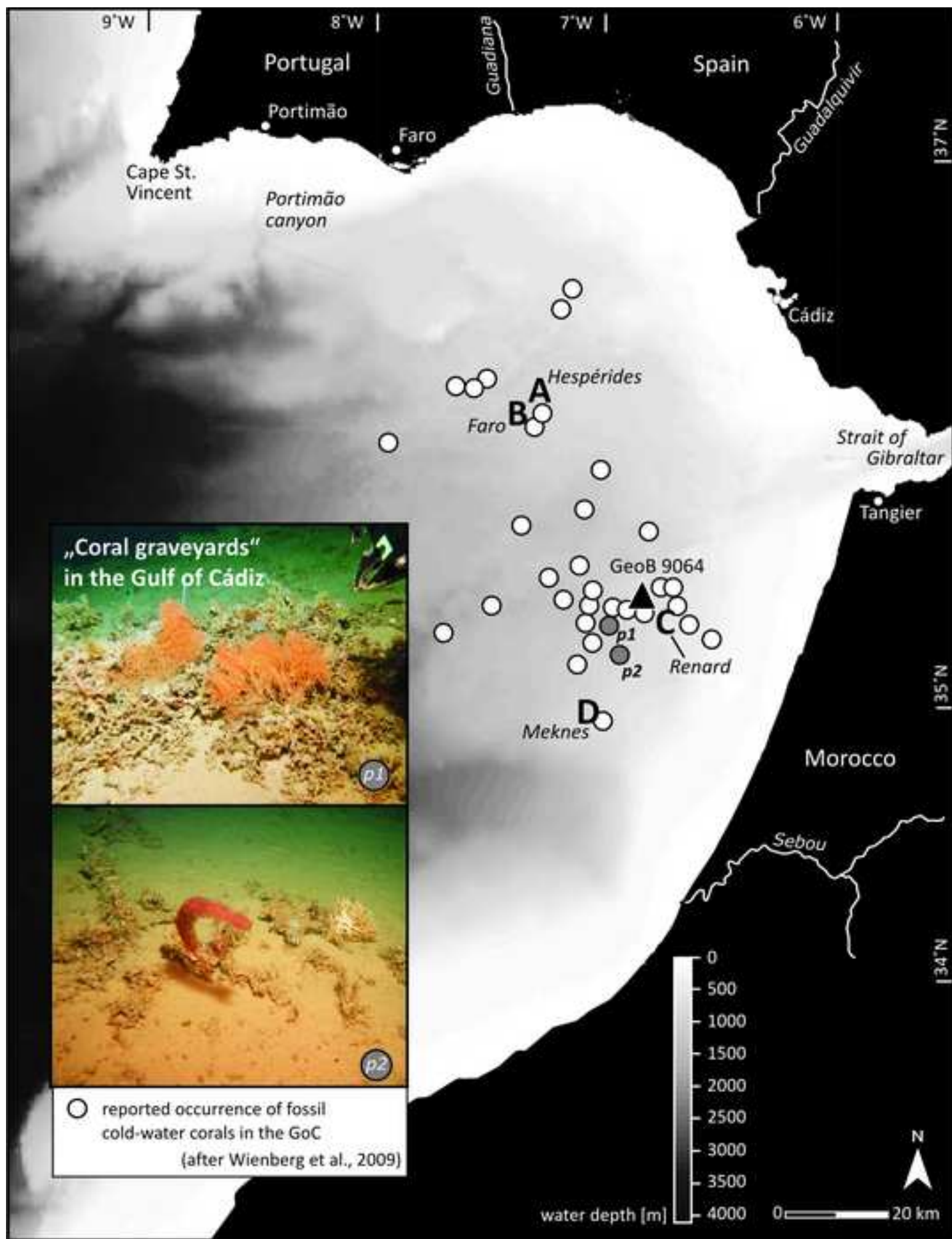**Click here to download high resolution image**
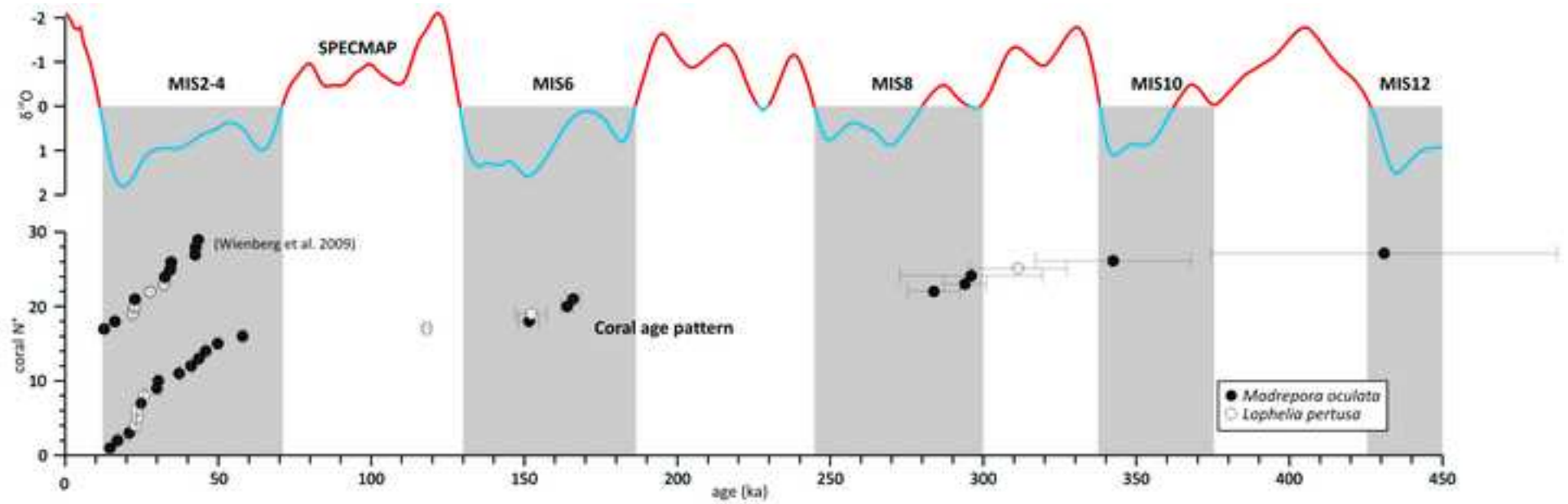
Figure2
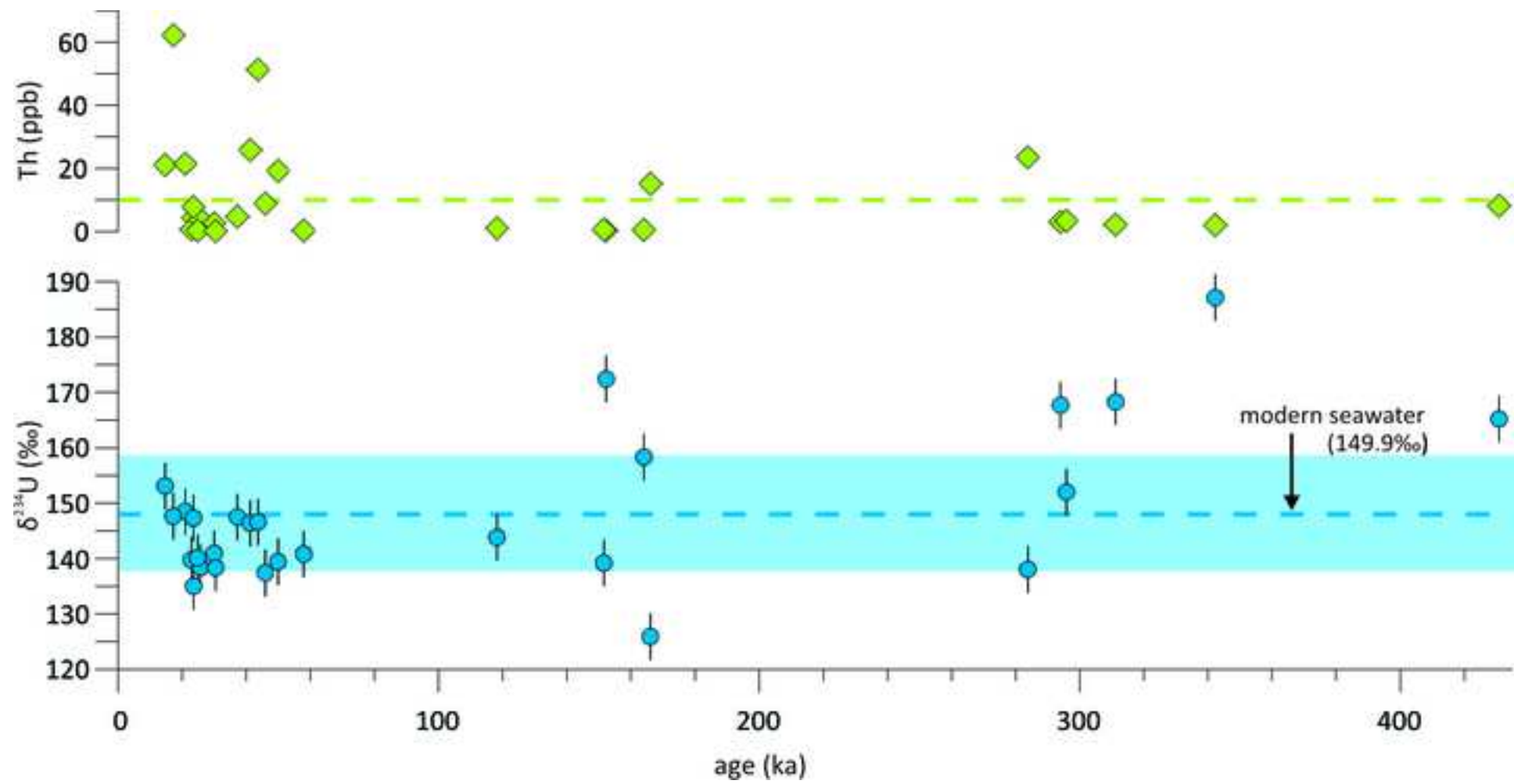
Figure3
Click here to download high resolution image
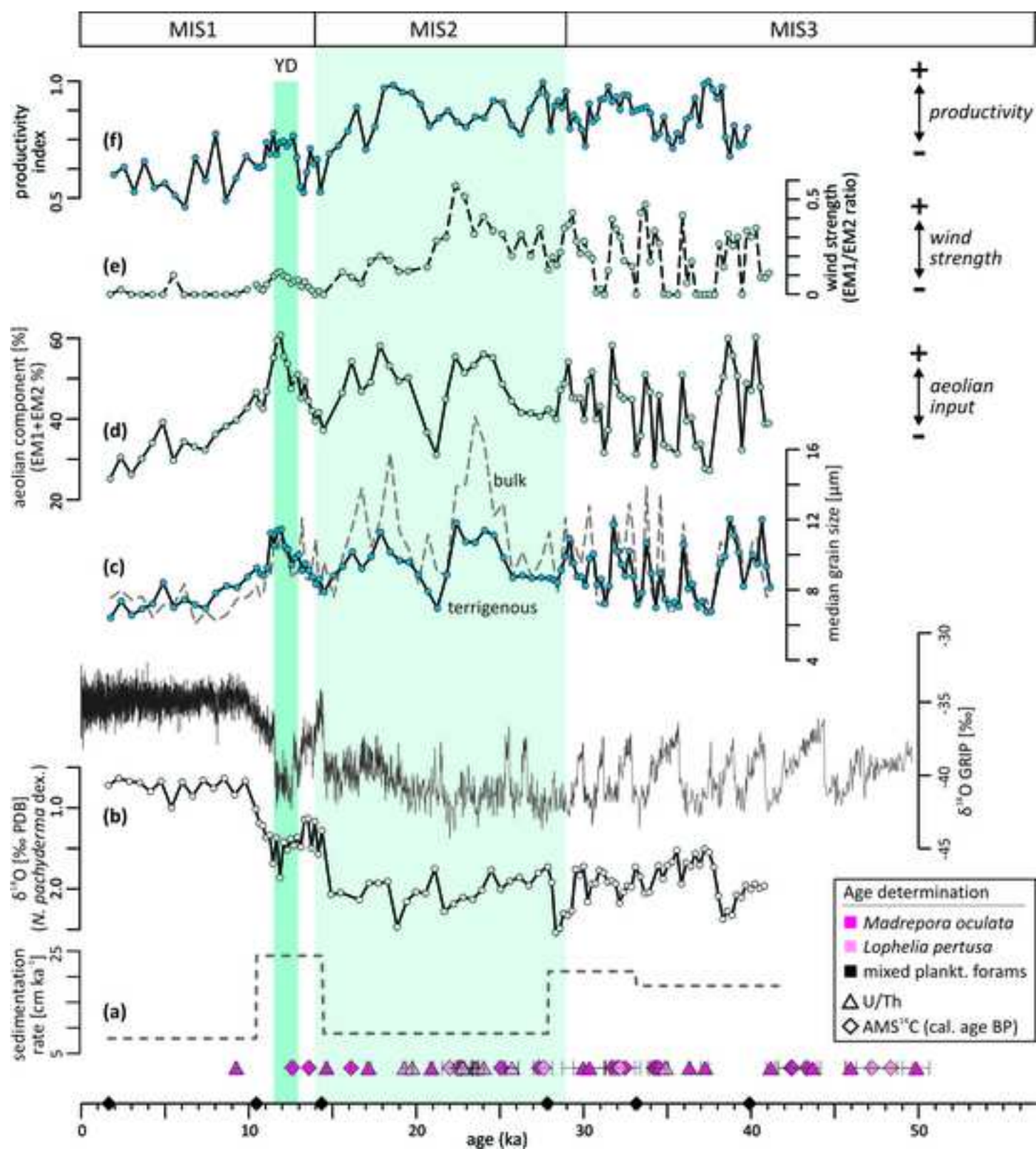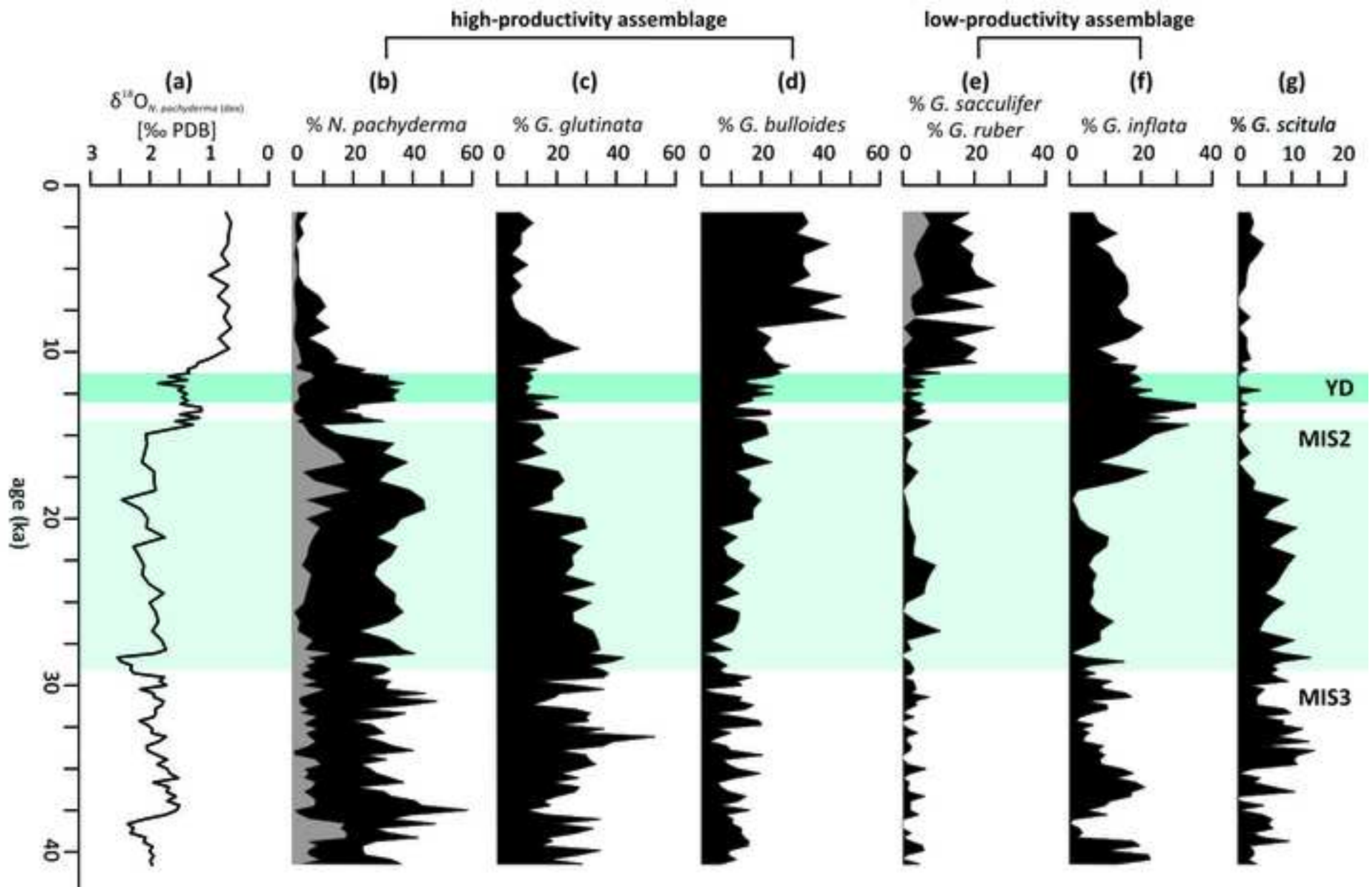
Figure4

Figure5
Click here to download high resolution image

1 **Table 1.** Metadata of coral-bearing sediment cores collected from various sites in the Gulf of

2 Cádiz (indicated in Figure 1 as A, B, C, D). Abbreviations: Lat, latitude; Lon, longitude; Wd,

3 water depth; Rec, recovery; Mv, mud volcano; Cm, coral mound; SM, Spanish margin; MM,

4 Moroccan margin; R, Ridge; PDE, Pen Duick Escarpment; Mo, *Madrepora oculata*; Lp, *Lophelia*

5 *pertusa*. Cruises: 1, RV *Sonne* cruise SO175; 2, RV *Maria S. Merian* MSM01-3; 3, RV *Pelagia*

6 cruise 64PE229.

			Cruise	Location	Core-ID	Lat (°N)	Lon (°W)	Wd (m)	Rec (cm)	Coral content
A	Mv	SM	1	Hespérides Mv	GeoB 9018	36°10.98'	07°18.37'	702	347	0-5 cm: dendrophylliids, 5-347 cm: solely Mo; strongly altered fragments.
B	Mv	SM	1	Faro Mv (lower flank)	GeoB 9031	36°05.75'	07°23.28'	897	484	0-160 cm: Mo-dominated; strongly altered fragments.
	Mv	SM	1	Faro Mv (top)	GeoB 9032	36°05.55'	07°23.57'	843	220	0-60 cm: Mo-dominated, 60-220 cm: mud breccia.
C	Cm	MM	1	W Renard R	GeoB 9070	35°22.00'	06°51.90'	594	560*	0-560 cm: Mo and Lp.
	Cm	MM	2	W Renard R	GeoB 12104	35°21.99'	06°51.90'	590	523	0-523 cm: Mo and Lp
	Cm	MM	2	Renard R	GeoB 12102	35°21.11'	06°50.96'	585	518	0-518 cm: Mo, Lp, and dendrophylliids.
	Cm	MM	2	Renard R	GeoB 12103	35°21.18'	06°50.90'	591	568	0-568 cm: Mo and Lp.
	Cm	MM	2	PDE	GeoB 12101	35°18.88'	06°48.08'	545	468	0-468 cm: Mo, Lp, and dendrophylliids.
	Cm	MM	3	PDE	M2004-02	35°17.68'	06°47.25'	523	861	0-861 cm: Mo, Lp, and dendrophylliids.
D	Cm	MM	2	N of Meknes Mv	GeoB 12106	34°59.49'	07°04.56'	758	303	30-303 cm: Mo and Lp.

7
8 * the uppermost 40 cm of core GeoB 9070 were disturbed due to coring operation, thus the undistorted core
   depth ranges from 40 to 600 cm
9

Table 2. Ages, isotope concentrations and ratios (n.a., not available).

N°	Sample ID	Depth (cm)	Coral	Labcode	Age (ka)	± (ka)	^{238}U (ppm)	± (ppm)	^{232}Th (ppb)	± (ppb)	δ^{234}U(M) (‰)	± (‰)	δ^{234}U(0) (‰)	± (‰)
	1	*2*	*3*	*4*	*5*		*6*		*7*		*8*		*9*	
01	GeoB 9018	3	Mo	n.a.	**14.65**	0.09	4.020	0.004	21.019	0.052	149.8	1.9	156.1	2.0
02	GeoB 9018	123	Mo	n.a.	**294.00**	7.00	4.329	0.004	3.021	0.006	73.1	1.4	167.7	3.3
03	GeoB 9018	272	Mo	n.a.	**283.80**	8.50	4.005	0.004	23.536	0.064	61.9	1.5	138.0	3.3
04	GeoB 9031	10	Mo	n.a.	**20.92**	0.12	4.956	0.005	21.400	0.055	139.9	1.8	148.5	1.9
05	GeoB 9031	93	Mo	n.a.	**37.25**	0.23	5.263	0.007	4.796	0.009	132.8	2.3	147.5	2.5
06	GeoB 9031	150	Mo	n.a.	**45.94**	0.33	4.338	0.004	8.875	0.016	120.6	1.4	137.4	1.6
07	GeoB 9032	20	Mo	n.a.	**17.15**	0.15	4.447	0.005	62.092	0.192	140.6	1.6	147.6	1.7
08	GeoB 9032	47	Mo	n.a.	**41.17**	0.25	4.512	0.005	25.841	0.070	130.3	1.8	146.4	2.0
09	GeoB 9070	47	Lp	n.a.	**23.50**	0.12	4.622	0.003	4.428	0.010	137.9	1.1	147.3	1.2
10	GeoB 9070	298	Mo	n.a.	**43.68**	0.28	3.552	0.003	51.216	0.079	129.6	1.8	146.6	2.0
11	GeoB 9070	520	Mo	n.a.	**166.00**	2.40	3.968	0.004	15.089	0.033	78.7	1.7	125.9	2.7
12	GeoB 12101	57	Mo	Gif-1525	*not dateable*		3.085	0.004	0.351	0.002	59.5	3.2	/	/
13	GeoB 12101	146	Lp	Gif-1389	*not dateable*		3.214	0.004	0.920	0.003	47.4	3.0	/	/
14	GeoB 12101	451	Mo	Gif-1527	**430.76**	56.55	2.589	0.002	8.092	0.026	48.9	3.3	165.2	3.3
15	GeoB 12102	28	Mo	Gif-1529	**57.96**	0.74	4.390	0.005	0.316	0.001	119.5	2.7	140.8	2.7
16	GeoB 12102	166	Lp	Gif-1528	**118.16**	1.10	4.220	0.003	1.075	0.003	103.0	1.9	143.8	1.9
17	GeoB 12102	238	Lp	Gif-1390	**152.27**	5.12	3.035	0.003	0.306	0.003	112.1	2.9	172.4	2.9
18	GeoB 12102	376	Mo	Gif-1388	**151.56**	3.37	3.614	0.003	0.491	0.002	90.7	3.0	139.2	3.0
19	GeoB 12102	493	Mo	Gif-1386	**164.02**	2.01	3.194	0.003	0.495	0.002	99.5	1.8	158.3	1.8
20	GeoB 12103	34	Lp	Gif-1530	**22.88**	0.38	3.881	0.004	0.636	0.003	131.0	2.0	139.8	2.0
21	GeoB 12103	88	Lp	Gif-1392	**25.72**	0.39	4.462	0.006	3.873	0.010	128.7	2.9	138.4	2.9
22	GeoB 12103	200	Mo	Gif-1531	**29.98**	1.26	3.610	0.004	2.644	0.011	129.4	3.3	140.9	3.3
23	GeoB 12103	317	Mo	Gif-1532	**30.43**	0.96	3.828	0.004	0.192	0.003	126.9	2.2	138.3	2.2
24	GeoB 12103	444	Mo	Gif-1533	**49.85**	0.80	3.693	0.005	19.205	0.071	121.1	2.4	139.4	2.4
25	GeoB 12104	8	Lp	Gif-1387	**23.57**	0.18	4.435	0.003	7.778	0.016	126.3	1.7	135.0	1.7
26	GeoB 12104	373	Lp	Gif-1534	**311.20**	15.74	3.658	0.003	2.161	0.012	69.8	2.2	168.3	2.2
27	GeoB 12104	491	Mo	Gif-1535	**342.29**	25.38	3.492	0.004	2.003	0.008	71.1	2.6	187.1	2.6
28	GeoB 12106	117	Mo	Gif-1391	**295.86**	23.27	3.421	0.004	3.421	0.004	65.9	2.8	152.0	2.8
29	M2004-02	49	Mo	Gif-1631	**9.15**	0.71	3.512	0.011	0.103	0.014	149.3	3.0	153.2	3.0
30	M2004-02	85	Lp	Gif-1632	**19.36**	0.54	3.943	0.007	0.625	0.008	138.8	2.5	146.6	2.5
31	M2004-02	105	Lp	Gif-1633	**19.87**	0.52	3.284	0.010	0.695	0.006	136.0	3.9	143.9	3.9
32	M2004-02	141	Lp	Gif-1634	**21.37**	0.42	3.862	0.007	4.666	0.013	136.5	2.3	145.0	2.3
33	M2004-02	147	Lp	Gif-1635	**22.75**	0.26	4.016	0.006	2.209	0.006	133.0	2.9	141.8	2.9
34	M2004-02	176	Lp	Gif-1636	**24.03**	0.26	3.921	0.008	11.534	0.031	131.4	3.3	140.6	3.3
35	M2004-02	247	Lp	Gif-1637	**34.90**	0.43	3.099	0.004	0.310	0.001	130.3	2.5	143.8	2.5
36	M2004-02	273	Mo	Gif-1638	**36.27**	0.43	3.804	0.008	3.049	0.008	124.5	1.6	138.0	1.6
37	M2004-02	313	Lp	Gif-1639	**142.08**	1.92	4.068	0.010	2.908	0.009	96.6	2.3	144.4	2.4
38	M2004-02	343	Lp	Gif-1640	**175.01**	2.79	3.846	0.005	14.820	0.026	85.3	2.5	139.9	2.5
39	M2004-02	363	Mo	Gif-1641	**242.07**	8.35	3.174	0.008	0.506	0.003	85.4	2.7	169.3	2.7
40	M2004-02	403	Lp	Gif-1642	**262.80**	7.46	3.126	0.007	3.116	0.007	74.2	2.9	155.9	2.9

NOTE: *Column 1: S*ample label. **C**olumn **1** *: S*ample label. **Column 2***:* Depth in core. **Column 3**: Reef-forming scleractinian cold-water coral species, Lp *Lophelia pertusa*, Mo *Madrepora oculata*. **Column 4**: Labcode (not available for datings conducted at IFM-GEOMAR, N° 1-11). **Column 5**: Calculated coral ages. **Column 6**: ^{238}U concentration. **Column 7**: ^{232}Th concentration. **Column 8**: Measured ^{234}U/^{238}U activity ratios (δ^{234}U(M)) are presented as deviation per mil (‰) from the equilibrium value. **Column 9**: Decay corrected ^{234}U/^{238}U activity ratios (δ^{234}U(0)) are calculated from the given ages and with λ_{234U}: 2.8263x10^{-6} yr^{-1}. Note that ages are strictly reliable having values between 146.6‰ and 149.6‰ (modern seawater), reliable with values of 149±10‰, unreliable with values >149±10‰ (see also Stirling et al., 1998; Robinson et al., 2004; Esat and Yokoyama, 2006).

19   **Table 3.** AMS ^{14}C dates determined on multi-species samples of planktonic foraminifera

20   from sediment core GeoB 9064. The AMS ^{14}C ages were corrected for ^{13}C and a mean ocean

21   reservoir age of 400 years, and were converted to calendar years using the CALPAL 2007

22   Hulu software. Estimated sedimentation rates for core GeoB 9064 are supplemented.

Core depth (cm)	Labcode	Conventional age ^{14}C age (years)	± error	CALPAL age 1σ (68%) (calendar years B.P., P.=AD 1950)	± error	Sedimentation rate (cm kyr^{-1})
GeoB 9064						
4	Poz-20282	2 095	30	1 630	50	-
74	KIA-10065	9 665	60	10 430	100	7.95
169	KIA-13060	12 660	80	14 370	240	24.11
289	KIA-23840	23 440	180	27 860	190	8.90
399	KIA-29420	29 020	320	33 090	420	21.03
524	KIA-35660	35 260	630	39 960	960	18.20

23